UAB
Universitat Autònoma de Barcelona

Dipòsit digital de documents de la UAB

This is the **accepted version** of the journal article:

Yang, Hyunsoo; Valenzuela, Sergio O.; Chshiev, Mairbek; [et al.]. «Two-dimensional materials prospects for non-volatile spintronic memories». Nature, Vol. 606, issue 7915 (June 2022), p. 663-673. DOI 10.1038/s41586-022-04768-0

This version is available at https://ddd.uab.cat/record/269764

under the terms of the license

Two-dimensional Materials Prospects for Non-volatile Spintronic Memories

Hyunsoo Yang[1,*], Sergio O. Valenzuela [2,3,*] Mairbek Chshiev[4,5], Sébastien Couet[6], Bernard Dieny[4], Bruno Dlubak[7], Albert Fert[7], Kevin Garello[4,6], Matthieu Jamet[4], Dae-Eun Jeong[8], Kangho Lee[9], Taeyoung Lee[10], Marie-Blandine Martin[7,11], Gouri Sankar Kar[6], Pierre Sénéor[7], Hyeon-Jin Shin[12] and Stephan Roche[2,3,*]

[1]Department of Electrical and Computer Engineering, National University of Singapore, 117576 Singapore

[2]Catalan Institute of Nanoscience and Nanotechnology (ICN2), CSIC and BIST, Campus UAB, Bellaterra, 08193 Barcelona, Spain

[3]ICREA, Institució Catalana de Recerca i Estudis Avancats, 08010 Barcelona, Spain

[4]Univ. Grenoble Alpes, CEA, CNRS, SPINTEC, 38000, Grenoble, France

[5]Institut Universitaire de France (IUF), 75231, Paris, France

[6]IMEC, Kapeldreef 75, 3001 Heverlee, Belgium

[7]Unité Mixte de Physique, CNRS, Thales, Université Paris-Saclay, 91767 Palaiseau, France

[8]R&D Center, Samsung Electronics Co., Hwasung, South Korea

[9]Foundry Business, Samsung Electronics Co., Giheung, South Korea

[10]GLOBALFOUNDRIES Singapore Pte. Ltd., 738406 Singapore

[11]Thales Research and Technology, 91767 Palaiseau, France

[12]Inorganic Material Lab., Samsung Advanced Institute of Technology (SAIT), 16678, South Korea

*corresponding authors

Non-volatile magnetic random access memories such as spin-transfer torque (STT)-MRAM and next generation spin-orbit torque (SOT)-MRAM are emerging as key enabling low-power technologies, which are expected to spread over large markets from embedded memories to the Internet of Things. Concurrently, the development and performances of devices based on two-dimensional (2D) van der Waals heterostructures bring ultra-compact multilayer compounds with unprecedented material-engineering capabilities. Here, we first provide an overview of the current developments and challenges in the field, and then outline the opportunities which can arise by implementing 2D materials into spin-based memory technologies. We highlight the fundamental properties of atomically smooth interfaces, the reduced material intermixing, the crystal symmetries and the proximity effects as the key drivers for possible disruptive improvements for MRAM at advanced technology nodes.

Emerging technologies generally follow a hype cycle before reaching the mature production stage. When NAND Flash memory was first commercialized in 1989, it competed against conventional non-volatile memories such as electrically erasable programmable read-only memory (EEPROM)[1]. Even when its market size reached over $1.8B in 1995, the semiconductor industry was still uncertain about the full potential of this technology. However, new applications such as MP3 players and smart phones, which rapidly increased end-use demands, fuelled NAND Flash development to reduce cost per bit, resulting nowadays in 3D NAND Flash innovation[2]. Mobility and miniaturization trends in consumer electronics have continuously driven the NAND Flash market, which reached over $50B in 2020.[3] On the other hand, while their potential in terms of low power and speed is proven, spintronic memories are still emerging in terms of market size. The most advanced emerging generation of MRAM, based on spin-transfer torque mechanism (Fig. 1), is already addressing a few market segments. However, it is envisioned that, in the near future, the MRAM market will expand significantly by addressing the power and data-transfer (memory-wall bottleneck) challenges in a variety of embedded applications, including neural networks and in-memory computing[4,5]. Considering that the embedded emerging non-volatile memory market is forecasted to grow from $20M in 2019 to $2.5B by 2025,[6] it could well drive MRAM growth, as mobile consumer electronics has driven NAND Flash in the past. In order to achieve such a growth, MRAM technology will meet a variety of challenges requiring material and device integration breakthroughs, in which two-dimensional materials (2DMs) could play a key role.

Indeed, since the discovery of graphene, followed by an ever-growing family of related materials[7], 2DMs have emerged as potential enablers for potentially ultra-compact device architectures or radically new concepts for spin information processing[8,9]. Scientific advances of 2DM-based spintronic devices as well as recent progress in large-scale co-integration of

2DMs with conventional microelectronics materials[10,11], open a promising perspective for developing innovative MRAM technology.

Here, we provide an overview of the most recent developments, identify challenges and opportunities brought by 2DMs for MRAM and give a vision about how progress in 2DMs research could morph into a game changing solution for future generations of spintronic memory technologies. We first describe fundamental MRAM concepts and the prospects for MRAM commercialisation, including the main roadblocks for broader deployment. We then highlight the unique opportunities brought by 2DMs and van der Waals (vdW) heterostructures to overcome some of the technological challenges. Afterwards, we analyse the requirements and challenges for further advances concerning growth, processing, and integration of 2DMs to enable an impact in next generation spintronic-memory development. Finally, an outlook provides a vision of 2DM-MRAM technologies.

STT-MRAM and next generation SOT-MRAM

Non-volatile MRAM technologies are built on magnetic tunnel junctions (MTJ) comprised of two ferromagnetic (FM) layers separated by a thin insulator. One of the FM layers, known as the free layer (FL), stores information, while the other, the reference layer (RL), provides a stable reference for reading the FL information. Two main technologies relying on electrically generated spin-currents have emerged to control the FL magnetization: spin transfer torque (STT)[12] and spin orbit torque (SOT)[13].

The STT concept was first introduced in 1996[14,15] and implemented at STT-MRAM chip level in 2005[16]. STT is observed in a two-terminal geometry, in which a vertical current is injected through the MTJ (Fig. 1a). The current tunnelling through the barrier is spin-polarized, leading to the FL magnetization reversal for large enough currents, due to the transfer of angular momentum. The relative magnetization orientation of the FL and RL layers

determines the resistance of the device, which is monitored by the tunnelling magnetoresistance (TMR).

SOT-MRAM is based on three-terminal devices, where an additional conducting path is added adjacent to the FL (Fig. 1b). A charge current flowing through this path results in the injection of a spin-polarized current into the FL in virtue of the spin-Hall and/or Rashba-Edelstein effect[13,17-19]. In such devices, SOT can switch the FL magnetization without passing a current through the MTJ tunnel barrier. At the expense of adding another terminal, the decoupling of the write and read current paths prevents write errors during read operation and reduces the risk of voltage breakdown. It further enables versatile cell designs by allowing the spin torque direction to be set independently of the anisotropy direction in the stack[20]. Using SOT, magnetization switching has been observed in the ps time scale[21].

Commercialization and challenges of spin memory

Successful commercialization of STT-MRAM in solid-state drives (SSD) and wearable electronics (Box 1) has been achieved after several major breakthroughs in MTJ technologies[22], including enhanced STT-switching efficiency and TMR amplitude, interfacial perpendicular magnetic anisotropy (PMA) at magnetic metal/oxide interfaces[23-25], synthetic antiferromagnets (SAF), the suppression of etch-induced sidewall re-deposition and reduction in process variability (Fig. 2). To cover a broader range of envisioned applications (Box 1), further development of cost-effective and versatile MRAM technology will be crucial. It will also be necessary to ensure proper downscaling to maintain competitiveness at advanced technology nodes, in particular regarding MTJ diameter and cell-to-cell pitch. For example, because of the required analog circuitry, as a rule of thumb it is desirable to keep the STT-MRAM bitcell about 3 times smaller than the SRAM cell size at a given technology node so that the benefit is worth the technology change.

Improving the MTJ stacks and their versatility using conventional materials and integration processes is a difficult challenge. The actual stacks consist of dozens of ultra-thin layers (Fig. 1) in which each material and interface plays an important role in determining the device performance (Fig. 2). Below, we discuss some of these important aspects. In terms of materials, modern MRAMs rely on the crystalline MgO tunnel barrier, while the FM layers that are in contact with MgO are typically made of crystalline CoFeB (Fig. 2a). The CoFeB/MgO/CoFeB combination is attractive because of its high TMR ratio originating from the spin filtering effect in crystalline-MgO/FM, as predicted in 2001[26] (Fig. 2b). The structure appears to be simple but practical devices are far more complex. The RL layer requires a much higher magnetic anisotropy than the FL to be stable during memory operation. For this purpose, almost all MRAMs use a multilayer SAF to pin the RL (Fig. 2c), which relies on strong antiferromagnetic coupling between two ferromagnetic layers, and gives rise to a magnetically hard structure.

Another crucial point is PMA[23-25] (Fig. 2d) because perpendicularly magnetized stacks have a better scalability than the in-plane magnetized counterparts. Due to the switching dynamics induced by STT, a better trade-off between the thermal stability of the FL magnetization and the write current is obtained in out-of-plane magnetized MTJs[27]. Interfacial PMA can originate from spin-orbit interactions deriving from electronic hybridization effects, magnetocrystalline anisotropy, and interfacial strain. PMA was demonstrated in a Ta/CoFeB/MgO structure[24] but requires very thin CoFeB, which results in increased damping from the spin pumping effect and less efficient STT, while the anisotropy strength is insufficient for small devices (< 30 nm). A solution for these issues involves double MgO barriers, such as MgO/CoFeB/MgO and MgO/CoFeB/Ta/CoFeB/MgO (Fig. 2d). Here, having the FL between two oxide barriers effectively increases the anisotropy[28,29], providing thermal stability of the magnetization down to ~20-nm cell diameter[30]. Other approaches to enhance

PMA below 20 nm rely on vertical shape anisotropy[31,32], but these concepts face manufacturing challenges due to the large MTJ aspect ratio.

As the MTJ size is downscaled, the TMR must remain high enough while an increase in the PMA is required to maintain thermal stability and data retention. However, the enhanced anisotropy of these structures forces the use of large current densities to achieve reliable magnetization switching, which increases energy consumption. As such, introducing voltage controlled magnetic anisotropy (VCMA) to assist or induce the switching could be helpful (Fig. 2e). It has been shown that a voltage across the MgO tunnel barrier results in charge accumulation near the FL/MgO interface, inducing atomic-orbitals occupancy changes that modulate the magnetic anisotropy[33-35]. VCMA-assisted writing could therefore reduce the energy dissipation and memory cell area by lowering the driving current. Unfortunately, the strength of the VCMA effect in CoFeB/MgO remains insufficient for practical implementations.

Pitch scaling also tends to increase the failure rate by forming shunting paths on the sidewall due to metallic re-deposition during MTJ patterning.[36] The physical and chemical damages on the pillar sidewall become even more problematic for downscaled MTJ devices. Broken symmetry of atomic bonding on the sidewall from physical bombardment or chemical diffusion of etching gases significantly degrades both the spin polarization and the magnetic anisotropy. Finally, another important issue is related to atomic intermixing at interfaces, taking place between the metallic layers in the MTJ during the post thermal annealing at ~400 °C required to improve the MTJ crystallinity and CMOS integration (Fig. 2f). When intermixing reaches the tunnel barrier, it leads to performance deterioration. This issue becomes more relevant as the thickness of the layers is reduced at advanced nodes, since the risk of failure of the tunnel barrier increases when the layer roughness becomes comparable to its thickness.

There are also various integration and material challenges associated to SOT-MRAM (Fig. 2g). SOT-MRAM uses the technological platform of STT-MRAM, thus knowledge and solutions developed for STT-MRAM could be transferable to SOT-MRAM development. However, a fundamental difference lies in the stack design. While in STT-MRAM the FL generally is on the top of the MTJ stack (bottom pinned, Fig. 1c) in SOT-MRAM, it is on the bottom (top pinned, Fig. 1d). This forces to re-design material growth protocols and to introduce specific seed layers to achieve the desired crystallinity of MTJs. Stacks with in-plane magnetization increase the SOT cell size, although they have the benefit of magnetic field-free switching. In contrast, for deterministic switching of perpendicular anisotropy SOT devices, an in-plane external magnetic field along the current direction is required (Fig. 2g). This magnetic field is a major hurdle for practical SOT-MRAM applications. Various solutions have been proposed to obtain field-free switching such as complex shapes[37,38], the use of in-plane MTJ[39] that limits scalability and speed, the insertion of an in-plane magnet below the SOT line increasing writing currents[40], or using antiferromagnetic heavy metal SOT lines[41]. Although a solution embedding a magnet in 12-inch wafer integration process was demonstrated[42], this solution comes at the expense of uniformity, cost, security, and MTJ stability.

Opportunities with 2DMs for MRAM

Major progress in spin-torque memory technologies have been achieved by material developments. However, to date, only a very limited number of optimal material combinations have been identified, in particular CoFeB/MgO has played a prominent role for nearly two decades since no alternative has been found yet. Consequently, MRAM technology faces severe constraints, threatening its future evolution and broad deployment. In recent years, wide varieties of novel emerging 2DMs and heterostructures have shown the potential to address the aforementioned issues and challenges. In a monolayer form, 2DMs are atomically thin and their interfaces are atomically smooth. They interact weakly, through vdW interaction, with

minimal element intermixing. In addition, given their atomically-thin nature, their properties could be tuned by external electric fields or proximity effects[9]. They exist in metallic, insulating, semiconducting, ferromagnetic and antiferromagnetic forms without or with broken crystalline symmetries, and presumably, they can be stacked in any preferred combination and order.

Therefore, the properties and versatility of 2DMs make them very attractive for spintronics and, in particular, for memory technologies, which strongly rely on ultrathin materials and their interfaces to harness the required functionalities (Fig. 2). Although 2DMs-based technologies are far from reaching the level of maturity of MgO/CoFeB based MTJs (for example the first 2D magnets were isolated in a monolayer form just a few years ago and are right now barely exceeding room temperature operation)[43-46] vdW heterostructures are taking an increasingly prominent role in spintronics research.

Interfacial PMA and synthetic antiferromagnets

As the MTJ size scales down, the energy barrier to switch the FL decreases, which in turn increases its bit-to-bit variation, hence degrading data retention[47]. In principle, intrinsic interfacial PMA (Fig. 2d) can be enhanced by using FM materials with large spin-orbit coupling[23]. However, the use of an amorphous FM alloy is preferred to achieve epitaxial crystallization of the MgO barrier upon annealing,[48] which constrains the selection of the FM material. Besides, increasing the spin-orbit coupling in the FL would increase the damping and the write current[23]. Accordingly, there is a crucial need for innovative material alternatives to enable STT-MRAM below 15-20 nm.

In this context, 2DMs have been investigated as promoters of large PMA. The combination of graphene with Co, Fe, and/or FePd has shown promising results[49-53]. For example, calculations show that the PMA of Co films coated by graphene (on one or both surfaces) is enhanced by up to 100% compared to the PMA of pure cobalt, reaching an upper value of ~2 mJ/m^2.[51] The critical thickness of Co at which the out-of-plane to in-plane

magnetization transition occurs (>13 ML or >2.6 nm) increases, as confirmed experimentally with graphene/Co/Ir(111) samples[50,51] (Fig. 2d). In comparison, the PMA of pure Co vanishes beyond 7 ML. Downscaling potential to a MTJ pillar diameter of 10 nm has been estimated when both Co surfaces are covered by graphene or for FePd/Graphene interfaces[54] (Fig. 2d). Interestingly, graphene also presents potential for implementing SAFs, as revealed by the strong antiferromagnetic exchange coupling across a graphene spacer in out-of-plane magnetized FM/graphene/FM structures (Fig. 2c)[51,52,55]. The integration of graphene-based FL in STT/SOT-MRAM could minimize the Dzyaloshinskii–Moriya interaction arising at Co/graphene interfaces[56], which has a detrimental effect on device switching performance[57-60].

Encapsulation and intermixing suppression

As the lateral dimension of MTJs shrinks, device morphology profiles become very rough and non-uniform. Chemical vapour based 2DMs embedded in the MTJs can help overcome fabrication challenges and improve the device morphology as the tunnel barrier thickness and lateral dimension downscale (Fig. 2). Their atomically thin, flexible and generally inert nature can minimize defects related to dangling bonds, interface states and interfacial alloy formation[61]. For example, graphene can be simultaneously used as a contact and heat dissipation layer and hBN as an encapsulation and insulating layer.

2DMs can suppress diffusion of atoms in MTJs. Intermixing reaching the tunnel barrier eventually leads to device performance deterioration. Graphene and hBN have a dense electron cloud structure and a low chemical reactivity due to their compact hexagonal honeycomb-lattice, making it difficult for even the smallest He atom to spread. For this reason, 2DMs have been heralded as atomically thin impermeable membranes[62,63] to prevent the oxidation and corrosion of metals[64,65] and allow novel processes for spintronics such as atomic layer deposition (ALD)[66,67]. Large area 2DMs uniformly grown by CVD can therefore be used as an encapsulating layer to protect patterned MTJ cells from the post thermal and inter-diffusion of

BEOL processes (Fig. 2f). Similarly, many organic materials (as used in OLED for instance) hold tailoring potential for spintronics[68], which 2DMs integration could unleash by stabilizing interfaces.

Thickness engineering of material spacers follow a trade-off relationship.[25,69,70] A thick spacer could provide suitable texture decoupling and diffusion barrier, but the magnetic coupling weakens. 2DMs could provide ideal spacers since the trade-off relationship can be efficiently optimized. Large-scale 2DMs grown by CVD on FMs[71-73] preserve interfaces with spin polarized metallic states even after exposure to oxidative conditions.[66,67,74,75] Graphene and hBN have demonstrated outstanding performance as atomic diffusion barriers down to the monolayer.[67,76,77] Notably, large-scale graphene growth on high magneto-crystalline anisotropy and low magnetic damping FePd $L1_0$ PMA ordered alloy was recently achieved[53].

Additionally, the oxidation issue of FMs usually forbids low-cost ambient/oxidative processes such as ALD, which are widely used in the microelectronics industry.[78,79] ALD based Al_2O_3 and MgO tunnel barrier integration in spin valves have been demonstrated[66,80,81], showing high quality coverage with conformal and layer-by-layer growth at the angstrom limit (Fig. 2f). This hints the potential of 2DMs to unlock processes (ALD, use of organics) with implications to oxidation-resistant and enabled low-cost approaches.

Alternative tunnel barriers

2DMs cover a wide range of electronic properties from metallic (TiS_2) and semimetallic (graphene, WTe_2, $MoTe_2$) to semiconducting (MoS_2, $MoSe_2$, WS_2, WSe_2, black phosphorous, etc) and insulating (hBN) and can also exhibit topological properties (Bi_2Se_3, Bi_2Te_3, WTe_2, $MoTe_2$).[82-84] 2D magnets such as CrI_3, $CrTe_2$, $Cr_2Ge_2Te_6$ and Fe_3GeTe_2 have been recently added to this family[43,85-88], offering great potential for the replacement of bulk FMs and, perhaps, TMR enhancement.

The demand for controlling the thickness of oxide tunnel barriers with atomic level

precision represents a serious challenge. The spintronics community is struggling to achieve and control ultra-thin MgO tunnel barriers with homogeneous thickness over a large scale.[89,90] The natural aptitude of 2DM tunnel barriers, which can be defined layer by layer with atomic precision, is one of the key advantages (Figs. 2b and 2f).[91-96] Nonmagnetic materials, such as graphene, hBN and transition metal dichalcogenides (TMDC) MoS_2 and WS_2, have been demonstrated as a tunnel barrier in MTJs, exhibiting novel band structures or hybridization spin filtering effects and leading to a sizeable TMR value up to 80% with predictions as high as 10^{12}%.[76,77,80,91,97-107] Experimental demonstration of the direct integration of graphene in TMR devices has been carried out in CMOS compatible processes (< 450 °C with large-scale CVD)[67]. Owing to the development of large-scale technologies, such as CVD, molecular beam epitaxy (MBE) and pulse laser deposition (PLD), other 2DMs have been investigated for MTJs[76,101,108-114].

It is important to note that theoretical *ab*-initio studies on CoFe/MgO/CoFe based MTJ have predicted TMRs[26] in the range of several 1000% whereas experimentally the room-temperature record is 604%, while the TMR in commercial products is ~200%.[115,116] This discrepancy is due to defects in the MgO tunnel barrier, lattice mismatch between MgO and FM, diffusion of boron or other elements towards the MgO barrier, etc. With 2DMs, the MTJ stack could be closer to the ideal one thanks to their high stability, suppressed diffusion, and well-defined interfaces, which would favour downscaling. For example, all-2D based MTJs comprising a 2D tunnel barrier and 2D magnetic layers could be envisioned (Fig. 2f). A TMR of 160% at low temperature has been reported in a MTJ entirely made of 2DMs (Fe_3GeTe_2/hBN/Fe_3GeTe_2), with PMA and a spin polarization exceeding 60% gate tunability[99]. Even a larger TMR was predicted in Fe_3GeTe_2-based MTJs for various vdW spacers[117].

Furthermore, the fact that 2DMs and their heterostructures are atomically thin promises less technological efforts to process them into functional devices, avoiding

technological steps such as planarization. They could further enable novel memory elements as alternatives to traditional MTJs (Fig. 2b). A low-temperature magnetoresistance as large as 19000% was observed in tunnel junctions of four-layer CrI_3, a layered insulating antiferromagnet[118,119], while a TMR up to 100000% was predicted for VSe_2[120].

Spin-orbit torques

Compared to SRAM, the stand-by power of SOT-MRAM is negligible, but projected write (< 75 fJ) and read energies (< 25 fJ) using state-of-art stacks must be reduced[121]. Reading is directly linked to the minimum current detectable by the sense amplifiers and stand-by power. For fast reading < 5 ns with ~150−200% TMR, the read current should be ~50−80 μA. Typical transistor current capabilities in sub-28 nm technology nodes with minimum footprint is on the order of 30-100 μA, while state-of-the-art perpendicular SOT-MRAM projects a critical write current of ~300 μA per bit cell[121,122]. Hence, to prevent CMOS from dominating the cell size, a straightforward way is to improve the SOT efficiency ξ, the conversion ratio between spin and charge currents, to $\xi > 1$, while heavy metal layers, such as Pt and W, yield $\xi = 0.1\text{-}0.5$ [122-124].

The integration of 2DMs provides appealing opportunities for SOT-MRAM. The large spin-orbit coupling and associated spin textures of 2DMs, including TMDCs and topological insulators (TIs), make them serious candidates for inducing large spin torques. The most studied TIs are the Bi_2Se_3 and $(Bi_{1-x}Sb_x)_2Te_3$ family of materials. The observation of large damping-like torques and the achievement of room-temperature magnetization switching confirms their potential for SOT-MRAM.[125,126] Because of the reduced crystal symmetry of some TMDCs, unconventional torque components are also expected. Of significant relevance, an out-of-plane damping-like torque can be induced by WTe_2 and $NbSe_2$[127,128] (Fig. 2g), which could enable field-free SOT switching in perpendicular SOT-MRAM. A pronounced SOT is expected not only from the bulk but also from the surface in topological Weyl semimetals.

Room-temperature magnetization switching in a regime of domain wall motion has been reported in WTe_2/Py and WTe_x/Mo/CoFeB heterostructures[127,129,130].

Magnetization switching by SOT was also achieved in hybrid 2D/3D systems. Such is the case of Fe_3GeTe_2 or $Cr_2Ge_2Te_6$ at low temperature using an adjacent heavy-metal layer[131-134]. Large SOTs have also been reported in Py/WS_2 and CoFeB/(MoS_2 or WSe_2) bilayers[135,136]. A modulation of the coercivity with currents has been reported in Fe_3GeTe_2/WTe_2[137], and SOT switching was observed up to the Curie temperature (~200 K) of Fe_3GeTe_2 in WTe_2 (12.6 nm)/Fe_3GeTe_2 (7.3 nm) with PMA[138].

Engineering and tuning material properties

The control of the magnetic anisotropy with electric fields (VCMA) provides an engineering knob to optimize the trade-off between data retention and writability as well as to reduce the energy consumption. In current MTJs using metalling FMs, electric fields only penetrate a few Angstroms into the film surface, limiting the efficiency to control the magnetic properties. In contrast, the 2D magnets magnetic properties, Curie temperature and magnetic anisotropy, and spin filtering thru MgO are largely tunable using external stimuli such as electric fields[87], strain[139-142] or light.

Another exciting aspect is to leverage on the asset of hybridization (proximity or interface effect)[9,68,92,143] that could allow spin filtering and resistance-area product reduction (< $\Omega\cdot\mu m^2$). In proximity with a FM, the large gap insulating hBN have already shown to become metallic leading to spin filtering and a TMR of 50% in an 2D-MTJ[76] . Similarly, for graphene it was also possible to reach a TMR of 80%.[77] Other 2DMs such as TMDCs (with specific thickness dependent band structure mechanisms) are now explored to further tailor spin selection at FM interfaces[101]. Finally, graphene can further increase the current at the boundary between large spin-orbit coupling material and the FM. Room-temperature, proximity-induced spin orbit coupling effects, which are tunable by gating, have been recently observed in

graphene/WS_2[144]. In combination with the proximity-induced effect, an enhanced spin torque could be obtained.

Material and integration challenges

Material challenges

MRAM is expected to progressively become mainstream in rapidly expanding areas such as IoT and Artificial Intelligence-based devices (Box 1) for which the development of cost-effective, downscaled MRAM technology will be essential[145]. However, the limited portfolio of the available state-of-the-art 3D materials and architectures could become an unsurmountable obstacle for the industry. In this regard, 2DMs offer unique opportunities; to advance their use, several notable challenges lie ahead that require material research and development, in hand with engineering efforts[146,147].

There are thousands of predicted stable 2DMs, including insulators, semimetals, magnets and novel electronic phases, such as Weyl semimetals or topological insulators[148-150]. Many of them have properties that make them potentially attractive for magnetic memory technologies. Substantial attention must therefore be directed towards identifying and characterizing the most promising candidates to optimize MRAM performance. MTJs incorporating 2DM tunnel barriers[92] currently present TMR values[77] that are already comparable to those of the first generation of crystalline MgO barriers[151] that later became technologically relevant devices[115,116]. This is reinforced by the added potential of the newly developed 2D magnets. While we cannot predict whether such a suitable 2DM for memories will be available anytime soon, we can highlight tremendous efforts by the community in this direction[43-46]. Indeed, considering that the first 2D magnets were reported in 2017[85,86] already observing 2D magnets with a Curie temperatures near room temperature is impressive and efforts are undergoing to achieve this objective, relying on new material sets, improved control and sample quality, and doping approaches.[152-157] Hence, despite the results being not yet

competitive for nowadays room temperature standards, the tremendous effort made by the community and the fast pace of progress made in the recent years (from tunnel barriers to 2D magnets) to target functional large-scale spin-based technologies allow to envision the possibility of functional large-scale spin-based technologies operating at room temperature in the not so distant future.

Reported SOT efficiencies with 2DMs, especially TIs, largely surpass those of heavy metals. Crystal-dependent symmetries for field-free switching and VCMA are phenomena not easily implemented in today's MRAM materials. However, most SOT studies use micron-scale devices, where magnetization switching may occur via mechanisms with low activation barriers, such as domain motion. Future research efforts are required to extend these studies to practical sub-100-nm devices. In hybrid systems, the reactivity between 3D transition metals and 2D chalcogenides changes the nature of the interface, which may form uncontrolled interfaces due to chemical reaction[158-161]. Alloys and magnetic dead layers can modify the underlying SOT mechanisms[160,161]. However, if mastered, hybridization could become an asset for moving toward ultra-compact geometries[68,160]. All-2D vdW heterostructure would provide an opportunity to control SOT phenomena and may help overcome diffusion issues.

Explorative experiments with 2DMs are typically carried out using micrometre-sized flakes exfoliated mechanically from bulk materials. This technique is not up-scalable. The development of 12-inch wafer-scale CMOS-compatible growth process (direct growth on process wafer or layer transfer, Fig. 3a) is thus necessary to address the scalability issue; this remains a critical challenge for any 2DM implementation in microelectronics[146,147]. Furthermore, follow-up integration processes will need to maintain the original structure and device performance of 2DMs (delamination risk elimination, surface treatments, low damage co-integration with MRAM stacks, Figs. 3b and 3c).

Large scale growth

Growth methods to obtain uniform 2D layers on large areas could be based either on chemical methods (e.g. CVD) or on physical deposition such as MBE, PLD, and sputtering[113,114,146,162-169] (Fig. 3a). Chemical routes are arguably the most promising thanks to their low cost and compatibility with large wafer processing but progress so far is limited to a few selected materials. Single-crystal graphene and hBN growth has been scaled beyond 6-inch wafer at over 1000 °C using CVD[170-172] although single-crystal growth remains to be achieved, polycrystalline graphene growth has been demonstrated at 450 °C with plasma CVD[173,174]. During CVD growth, precursors react in the vapour phase in the wafer surface (650 −1000 °C). A low nucleation rate leads to the formation of large isolated flakes of high crystalline quality, which cover only a very small fraction of the substrate, with randomly oriented domains and poor control of the number of layers. The use of less stable metal and chalcogen precursors in TMDCs growth reduces the growth temperature (300−560 °C) and increase the nucleation rate[175-177]. Precursor control growth could drastically reduce the thermal budget for the fabrication, which is a promising approach for direct growth in BEOL compatible wafers. Using this technique, monolayers of TMDCs are grown over a wafer scale, but they remain polycrystalline, which degrades their electrical properties.

Processing and integration

After the growth over large areas of high crystalline quality 2DMs, their transfer from the growth to the target substrate is required for further processing and device integration (Fig. 3b). In this respect, the technological challenge consists of maintaining the 2D layer integrity during the process. The most widely used approach is the polymer-assisted transfer, in which a polymer film is used to mechanically support the 2DM[178-180]. The release from the growth substrate could be achieved in a solution by electrochemistry, chemical dissolution of the substrate or simply intercalation of water between the substrate and 2DM. Recently, another transfer method called spalling has been developed where the 2DM is detached from the

substrate by the strain induced by a metallic film grown onto it[181,182]. The metal/2DM stack is then transferred onto the target substrate and the metallic film is chemically etched.

Although 2DMs are generally compatible with standard integration processes such as photolithography, etch, and deposition, significant process optimization would still be needed to maintain the original structure and properties of the 2DMs. Of particular relevance are reducing damage in plasma-based processes, increasing adhesion and suppressing material lifting in chemical processes, and patterning by etching in combination with selective stop techniques[183-187]. Another point of attention is to retain the original structure of 2DMs without self-deformation, degradation and interference with other layers. For instance, the deposition of a conventional MRAM stack is carried out using sputtering, which can expose the 2DM seed to a plasma that can easily damage the 2DM. Some solutions have been proved viable (off-axis, flipped chip)[188] and have to be adapted to large scale tools, such that the deposition condition can be modified to be damage-free (see Fig. 3c as an example) while not degrading magnetic properties and stack performances.

Outlook and roadmap

Today, a variety of memory technologies complement each other for computing, data storage, and embedded applications. Figure 4 outlines a roadmap for MRAM. STT-MRAM has been already commercialized for persistent memory in storage devices and servers as well as wearable electronics. MRAM is fostering key emerging markets, such as wearable, automobile, IoT, biosensor, various cache, and buffer memory applications. Its development over recent years has been astonishing and it is clear that it will shortly play a central role in the embedded non-volatile memory market.

However, the requirements of each application vary significantly as summarized in Table 1. Flash-replacement STT-MRAM requires high data retention (> 20 years) but accepts low endurance (10^6 cycles). In contrast, SRAM-replacement STT-MRAM requires high

endurance (> 10^{12} cycles) and high bandwidth but needs much less data retention, even down to a few seconds. One major challenge for automotive applications is reliable chip operation even under extreme environment such as a high temperature of 150 °C or exposure to external magnetic fields that can increase the bit error rate. Good read margin up to 150 °C and magnetic immunity to guarantee 10 years reliability were demonstrated[47,189,190]. Finally, both bit-cell size reduction and operation speed enhancement are key factors in order to expand into the SRAM-replacement area. Recently, a write/read speed less than 10 ns and 10^{12} cycling endurance was demonstrated[191] showing a promise for SRAM replacement. On the other hand, SOT-MRAM is still a topic of intense research and under industrial initial assessment[122-124]. In order to move forward, the first step is to establish the manufacturability using industrial CMOS compatible processes. In fact, SOT-MRAM was recently demonstrated up to 12-inch scales[42,122] with reliable sub-ns switching, low error rates and high endurance on Ta/CoFeB/MgO or W/CoFeB/MgO stacks using either perpendicular[42,192-194] or in-plane[39,195] magnetization.

It is however unknown how scaling beyond the 14-nm node will be achieved with conventional materials, when the MTJ feature size is projected to be below 30-40 nm (Fig. 4). Current technologies with bulk materials and conventional MgO–based MTJs will reach their limit in various fronts, including PMA and tunnel barrier roughness. Within this context, the development of 2DM-based spintronic devices has been spectacular, providing opportunities for technological progress. In particular, magnetization switching by SOT has been recently observed in stacks incorporating 2DMs[134] while practical VCMA could become a reality by taking advantage of their ultrathin, atomically smooth properties. Large-scale integration of 2DMs in a fab environment will be accelerated in the coming years by efforts such as the 2D Experimental Pilot Line (Fig. 4), which will be the first foundry to integrate graphene and layered materials into semiconductor platforms[196]. Therefore, it is natural to envision that the large family of 2DMs could frame the roadmap for future advances of non-volatile spin-torque

memory technologies. Many technical material and technical challenges remain. However, given the unprecedented speed at which progress is achieved and the high pace at which new 2DMs are discovered and characterized, we shall be optimistic for the forthcoming steps towards moving to higher technology readiness levels. This could not only potentially frame further commercial exploitation of 2DM-based non-volatile memory technologies, but also serve as pathfinders for exploration of spin-based logics and functionalized other spintronics devices[4,197].

Table. 1. Specification comparison for various MRAM applications. Target applications are indicated with brackets. Relevant 2DM technologies discussed in the main text are listed in the last column.

	STT (eFlash replacement)	STT (SRAM replacement)	SOT (SRAM replacement)	Relevant 2DM tech.
MTJ size	60-80 nm	30-50 nm	30-60 nm	PMA enhancement
TMR value	170-190%	180-200%	> 200%	2D tunnel barrier Stress barrier
Write speed	200 ns - 1 μs	< 10 ns	< 5 ns	2D spin source, gating, proximity
Read speed	20 ns	< 10 ns	< 5 ns	TMR enhancement
Retention	> 20 yr	10 s	10 s	PMA enhancement
Endurance	> 10^6 cycles	> 10^{12} cycles	> 10^{14} cycles	Stress/diffusion barrier, encapsulation layer

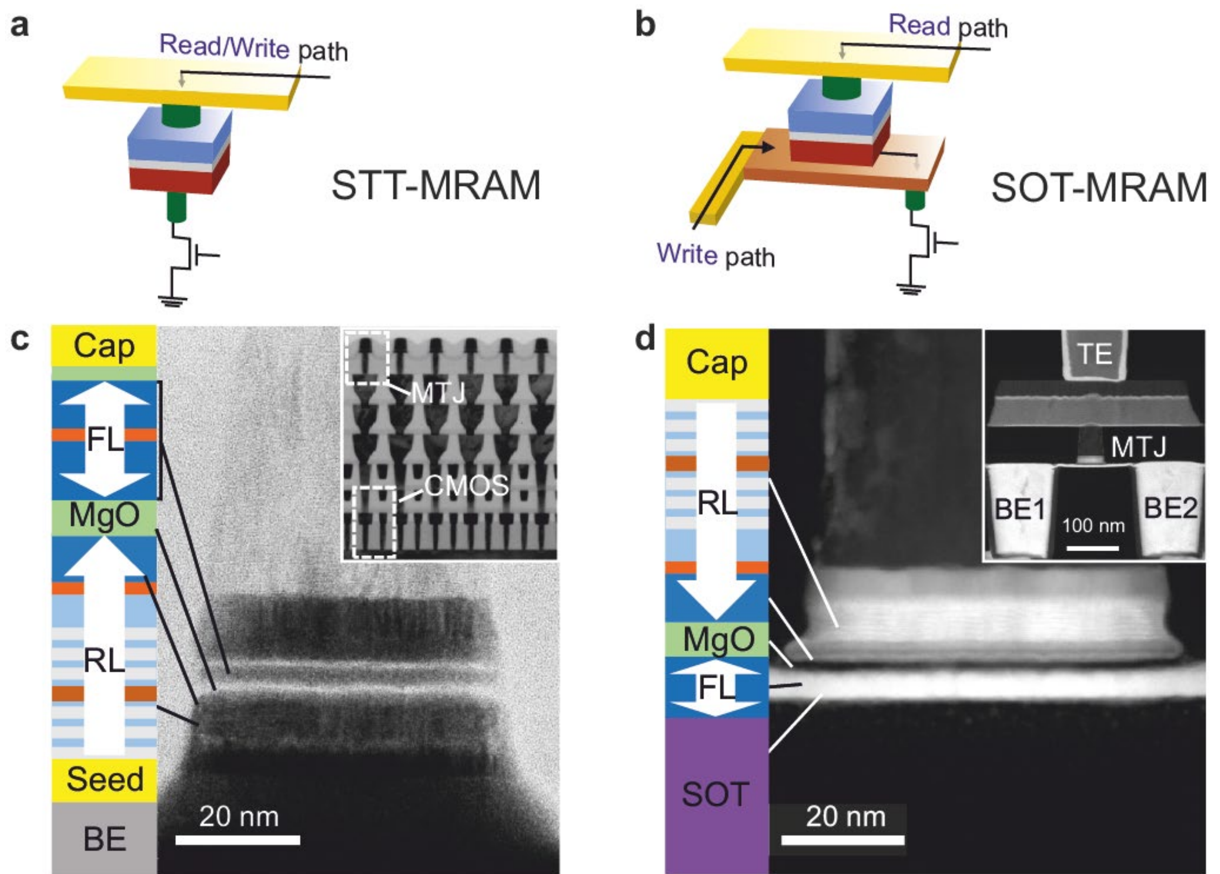

Fig. 1 | State-of-the-art MRAM technologies. a and **b,** Schematics of STT-MRAM and SOT-MRAM cells with perpendicular magnetic anisotropy (PMA), respectively. **c,** Bottom-pinned STT-MTJ sketch and transmission electron microscopy (TEM) cross section of 45 nm diameter STT-MTJ consisting of a CoFeB free layer (FL), MgO tunnel barrier and CoFeB/spacer/Co/Ru/[Co/Pt] reference layer (RL). The inset shows TEM cross section of STT-MRAM array (top dash box) controlled by CMOS (bottom dash box). **d**, Top-pinned SOT-MTJ sketch and TEM cross section of 60 nm SOT-MTJ. The inset shows a typical SOT-MRAM cell where the write current is injected from bottom electrode BE1 to BE2, and the read current from top electrode (TE) to BE2. Images from GlobalFoundries and IMEC.

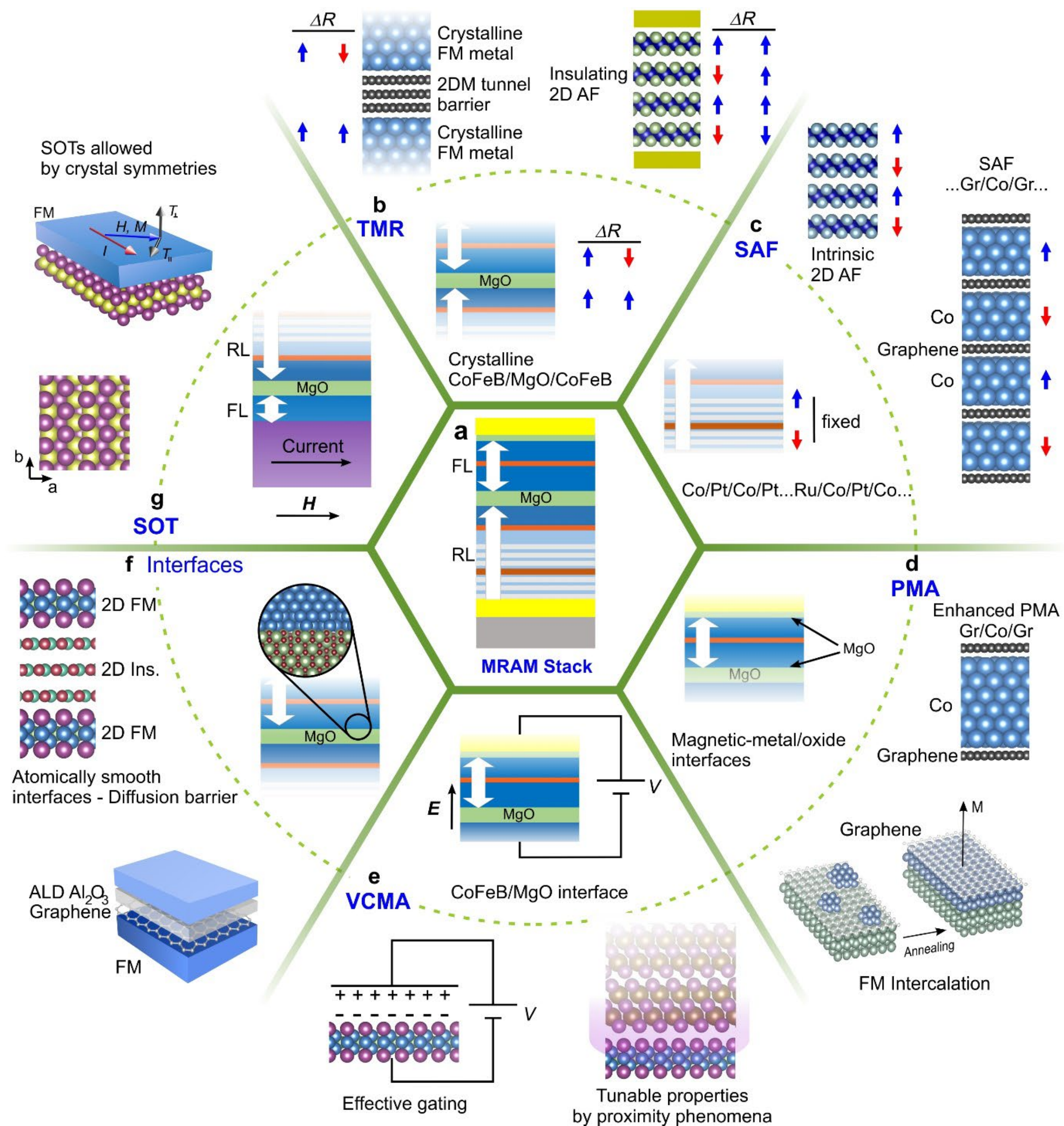

Fig. 2 | Fundamental phenomena of MRAM cells and 2DM prospects. Current solutions are represented inside the dashed circle**. a,** Typical STT-MRAM stack. FL and RL refer to the free and reference layer, respectively. The yellow top and bottom rectangles represent cap and seed layers, respectively. **b,** Tunnelling magnetoresistance (TMR). A change (ΔR) in the resistance is observed when the magnetization of FL switches, indicated by a switching from a blue to a red arrow. Modern MRAM technologies rely on coherent tunnelling across an MgO crystalline barrier. Similar performances are predicted with 2DM barriers (left). Large magnetoresistance has been observed in layered insulating antiferromagnets (right). **c,** Synthetic antiferromagnets (SAFs) are used to pin the magnetization of the RL. Equivalent magnetic structures are observed in layered materials (top) or can be artificially created (for example with Co/graphene, bottom). **d**, Interfacial perpendicular magnetic anisotropy (PMA) is found at the interface of magnetic metals and oxides but also on graphene/FM heterostructures. **e**, Voltage controlled magnetic anisotropy (VCMA) is observed at the interface of magnetic metals and oxides. Due to their atomically thin nature, 2DMs enable enhanced tunability of their properties, including gating and proximity effects. **f**, Intermixing and interface roughness becomes critical when scaling requires very thin (< 1 nm) tunnel barriers. This results in tunnel-barrier performance degradation and lack of reproducibility, which can be circumvented with atomically smooth 2DMs and 2DM diffusion barriers. **g**, For perpendicularly magnetized MTJs, an in-plane external magnetic field (*H*) along the current direction is typically required for switching. Low-symmetry 2DMs could help to eliminate the need for such a magnetic field.

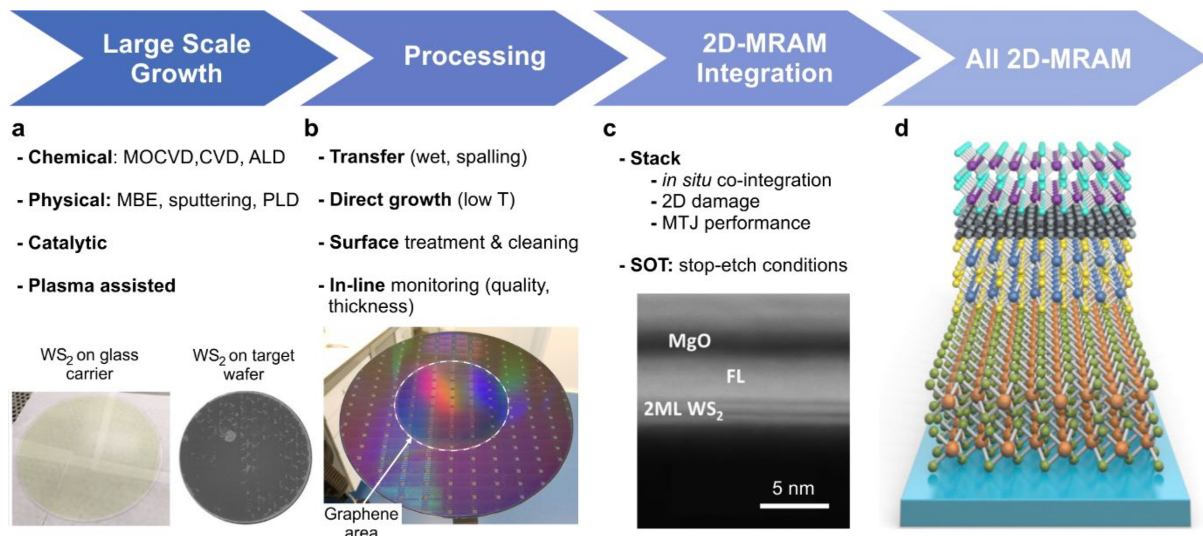

Fig. 3 | Challenges for integrating of 2DMs into MRAM technologies. **a,** Although significant progress has been achieved in small-scale demonstration, 2DM technology faces challenges in large scale growth of the materials for which several processes are being explored, from chemical, such as CVD, to physical such as sputtering and MBE (WS_2 on 300-mm glass carrier and target wafer is shown). **b,** Processing of 2D materials is under development, in particular regarding transfer and patterning of multilayers. For large-scale production, the development of suitable monitoring tools is also key. Graphene on a large wafer is shown. **c,** Integration in 2D-MRAM technologies. TEM cross section of top-pinned MTJ stack deposited on large scale grown 2DM (here WS_2) [ref.[198]], showing no degradation of WS_2. **d**, Potential implementation of 2DM in MRAM technologies as seed, tunnel barrier, FMs, encapsulation and SOT layers.

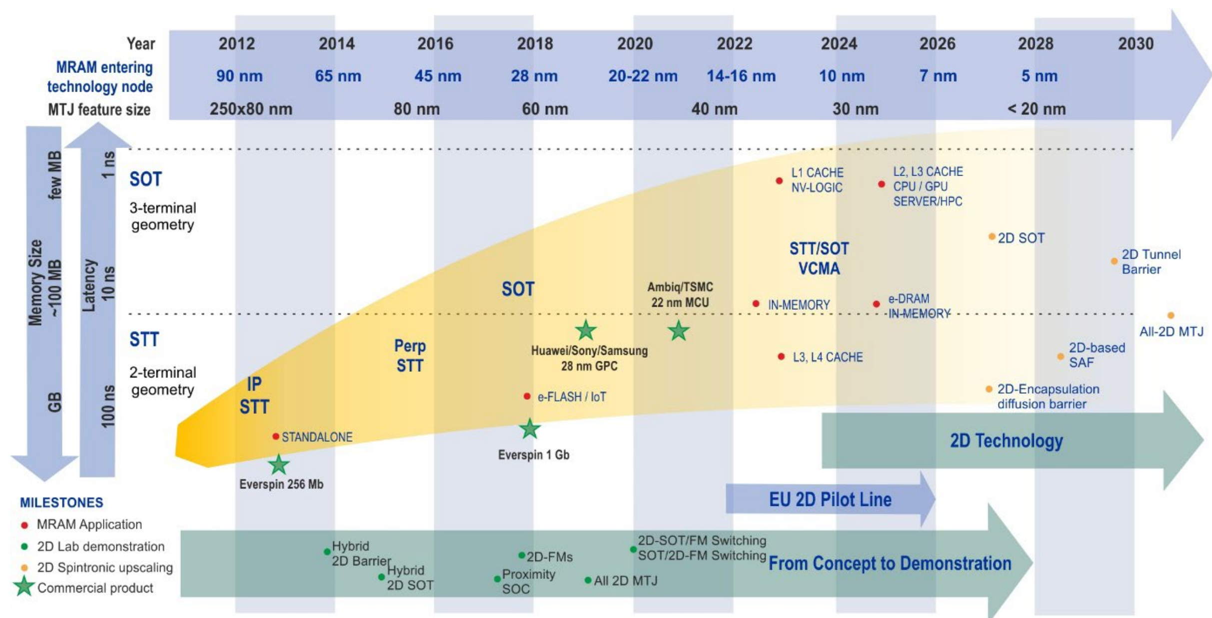

Fig. 4 | Spin torque memory technology roadmap. The projected feature size of the magnetic tunnel junction (MTJ) is shown at the top of the chart, together with the technology node at which a given MTJ size would be introduced. STT-MRAM offers non-volatility together with low power consumption, which is ideal for low-power microcontroller units (MCUs), wearables and IoT applications (Box 1). In terms of embedded non-volatile memory (eNVM) technology, eFlash scaling will likely reach its end at the 28/22nm node. STT-MRAM is also promising for automotive and SRAM replacement. Chipmakers and foundries started mass production for eFlash-type STT-MRAM in 2018 and started to develop SRAM-type applications for cache. SOT-MRAM can address high-speed and high-endurance applications such as cache and in-memory computing. The memory speed is best characterized by the latency time, which includes electrical time delays induced by routing from selector control to memory points and associated parasitic resistances and capacitances. As the memory size increases, the speed tends to decrease. Current MRAM technologies based on bulk materials are expected to reach their limits at about 20-nm MTJ feature size, after which 2DMs could play a key role to maintain MRAM downscaling. Actual 2DM milestones are shown at the bottom of the chart, including recent demonstrations of magnetization switching in heterostructures comprising 2DM-SOT materials and/or 2D FMs. Enabling 2DM-based technologies are indicated with STT and SOT technology projections and should be introduced at the indicated timelines to offset today's MRAM materials limitations. Efforts like the EU 2D Experimental Pilot Line are expected to accelerate the path to production (see Ref[196]). HPC stands for high-performance computing.

Box 1

MRAM markets and commercialization

STT-MRAM is the only non-volatile memory capable of high-density, high-endurance and fast-write operation and is considered as the best candidate for embedded non-volatile applications. The microcontroller units (MCU) market in 2020 was over $25B and will be driven by 5G internet of things (IoT), wearable, general-purpose MCUs and automotive electronics[199]. STT-MRAM can replace SRAM and NOR Flash in low-power MCUs, decreasing cost and power consumption. STT-MRAM is also promising for memory replacement in the automotive and biosensor sectors. There, embedded Flash (eFlash) is either not available or less cost-effective than embedded MRAM beyond the 28-nm node. SOT-MRAM is under development and their applications would be primarily as SRAM cache-memory replacement from L3/L4 to L2/L1 cache levels and registers in central (CPU) and graphical processing units (GPU). SOT-MRAM has also potential in non-volatile logic elements[200,201] and for in-memory computing.[202]

STT-MRAM has been released down to 28 nm, where eFlash technology co-exists. However, eFlash scaling is reaching its limits, while SRAM scaling becomes challenging due to stand-by leakage currents[203]. Applications include enterprise SSD, storage-class memory and wearable electronics. In 2017, Everspin shipped standalone 256Mb STT-MRAM using GLOBALFOUNDRIES (GFs) 40-nm technology[204] and started the production of 1Gb STT-MRAM at the 28-nm node[205]. TSMC has also developed a 22-nm technology, while Samsung Foundry commercialized in 2019 embedded STT-MRAM macro built upon low-power 28-nm fully depleted silicon-on-insulator (FDSOI) platform[206] (see Fig. 4). GFs has also delivered embedded STT-MRAM on its 22-nm FDSOI platform for IoT and automotive applications[207]. Embedded STT-MRAM is expected to expand in low-power wearable and RF applications, as demonstrated by Intel[208].

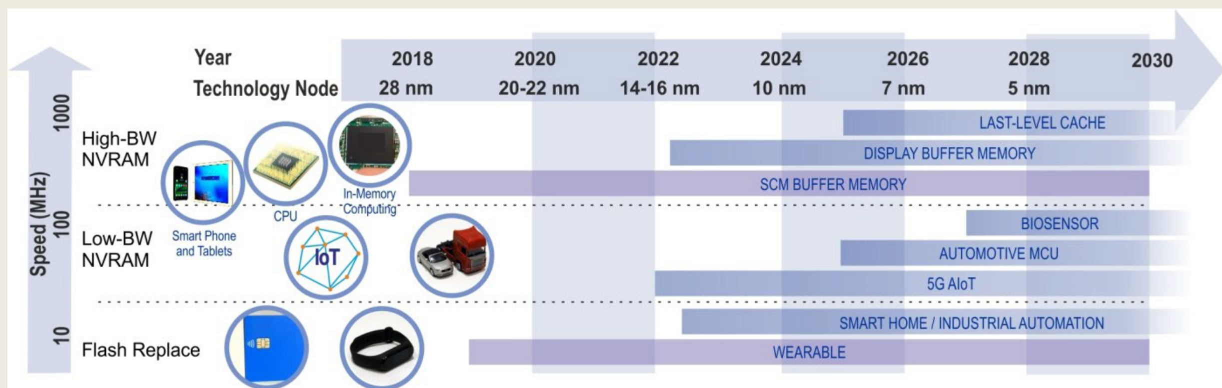

Box Fig. 1 | Potential markets. MRAM is considered as the only non-volatile memory with high-density, endurance and fast writing speed. Applications can be divided in three different categories: low-bandwidth (BW) non-volatile random access memories (NVRAM), high-BW NVRAM, and NOR Flash replacement. The MRAM memory cell is formed at the back-end-of-line (BEOL) without disturbing pre-established front-end processes (Fig. 1), which simplifies its implementation across multiple technology nodes. SCM stands for storage class memory and AIoT for artificial intelligence of things.

1 Yinug, F. The rise of the flash memory market: Its impact on firm behavior and global semiconductor trade patterns. *J. Int'l Com. & Econ* **1**, 137 (2008).

2 Park, K.-T., Byeon, D.-S. & Kim, D.-H. A world's first product of three-dimensional vertical NAND Flash memory and beyond. *14th Annual Non-Volatile Memory Technology Symposium (NVMTS)*, 14986230 (2014).

3 IC Insights. *DRAM Leads in Revenue, NAND With Top Percentage Growth in 2020*, <https://www.icinsights.com/news/bulletins/DRAM-Leads-In-Revenue-NAND-With-Top-Percentage-Growth-In-2020/> (2020).

4 Dieny, B. *et al.* Opportunities and challenges for spintronics in the microelectronics industry. *Nat. Electron.* **3**, 446-459 (2020).

5 Ikegawa, S., Mancoff, F. B., Janesky, J. & Aggarwal, S. Magnetoresistive random access memory: Present and future. *IEEE Trans. Electron. Dev* **67**, 1407-1419 (2020).

6 Yole Développement. *Emerging Non-Volatile Memory 2021*, <https://www.i-micronews.com/products/emerging-non-volatile-memory-2021/?utm_source=PR&utm_medium=email&utm_campaign=PR_EMERGING_NON_VOLATILE_MEMORY_YOLE_Market_Update_Feb2021> (2021).

7 Ferrari, A. C. *et al.* Science and technology roadmap for graphene, related two-dimensional crystals, and hybrid systems. *Nanoscale* **7**, 4598-4810 (2015).

8 Roche, S. *et al.* Graphene spintronics: the European Flagship perspective. *2D Mater.* **2**, 030202 (2015).

9 Sierra, J. F., Fabian, J., Kawakami, R. K., Roche, S. & Valenzuela, S. O. Van der Waals heterostructures for spintronics and opto-spintronics. *Nat. Nanotechnol.* **16**, 856–868 (2021).

10 Akinwande, D. *et al.* Graphene and two-dimensional materials for silicon technology. *Nature* **573**, 507-518 (2019).

11 Asselberghs, I. *et al.* Wafer-scale integration of double gated WS 2-transistors in 300mm Si CMOS fab. *IEEE International Electron Devices Meeting (IEDM)* **40.2**, 20548571 (2020).

12 Ralph, D. C. & Stiles, M. D. Spin transfer torques. *J. Magn. Magn. Mater.* **320**, 1190-1216 (2008).

13 Manchon, A. *et al.* Current-induced spin-orbit torques in ferromagnetic and antiferromagnetic systems. *Rev. Mod. Phys.* **91**, 035004 (2019).

14 Slonczewski, J. C. Current-driven excitation of magnetic multilayers. *J. Magn. Magn. Mater.* **159**, L1-L7 (1996).

15 Berger, L. Emission of spin waves by a magnetic multilayer traversed by a current. *Phys. Rev. B* **54**, 9353-9358 (1996).

16 Hosomi, M. *et al.* A novel nonvolatile memory with spin torque transfer magnetization switching: Spin-RAM. *IEEE InternationalElectron Devices Meeting (IEDM)*, 9071818 (2005).

17 Miron, I. M. *et al.* Perpendicular switching of a single ferromagnetic layer induced by in-plane current injection. *Nature* **476**, 189-193 (2011).

18 Liu, L. *et al.* Spin-torque switching with the giant spin Hall effect of tantalum. *Science* **336**, 555-558 (2012).

The above two papers first demonstrated SOT induced magnetization switching.

19 Pesin, D. & MacDonald, A. H. Spintronics and pseudospintronics in graphene and topological insulators. *Nat. Mater.* **11**, 409-416 (2012).

20 Fukami, S., Anekawa, T., Zhang, C. & Ohno, H. A spin–orbit torque switching scheme with collinear magnetic easy axis and current configuration. *Nat. Nanotechnol.* **11**, 621-625 (2016).

21 Jhuria, K. *et al.* Spin–orbit torque switching of a ferromagnet with picosecond electrical pulses. *Nat. Electron.* **3**, 680-686 (2020).

22 Aggarwal, S. *et al.* Demonstration of a reliable 1 Gb standalone spin-transfer torque MRAM for industrial applications. *IEEE International Electron Devices Meeting (IEDM)*, 19359435 (2019).

23 Dieny, B. & Chshiev, M. Perpendicular magnetic anisotropy at transition metal/oxide interfaces and applications. *Rev. Mod. Phys.* **89**, 025008 (2017).

24 Ikeda, S. *et al.* A perpendicular-anisotropy CoFeB–MgO magnetic tunnel junction. *Nat. Mater.* **9**, 721-724 (2010).

25 Worledge, D. *et al.* Spin torque switching of perpendicular Ta| CoFeB| MgO-based magnetic tunnel junctions. *Appl. Phys. Lett.* **98**, 022501 (2011).

26 Butler, W., Zhang, X.-G., Schulthess, T. & MacLaren, J. Spin-dependent tunneling conductance of Fe| MgO| Fe sandwiches. *Phys. Rev. B* **63**, 054416 (2001).

27 Apalkov, D., Dieny, B. & Slaughter, J. Magnetoresistive random access memory. *Proc. IEEE* **104**, 16317085 (2016).

28 Rodmacq, B., Auffret, S., Dieny, B. & Nistor, L. E. Three-layer magnetic element, magnetic field sensor, magnetic memory and magnetic logic gate using such an element. Patent US 8,513,944B2 (2013).

29 Sato, H. *et al.* Comprehensive study of CoFeB-MgO magnetic tunnel junction characteristics with single-and double-interface scaling down to 1X nm. *IEEE International Electron Devices Meeting (IEDM)*, 14062196 (2013).

30 Gajek, M. *et al.* Spin torque switching of 20 nm magnetic tunnel junctions with perpendicular anisotropy. *Appl. Phys. Lett.* **100**, 132408 (2012).

31 Watanabe, K., Jinnai, B., Fukami, S., Sato, H. & Ohno, H. Shape anisotropy revisited in single-digit nanometer magnetic tunnel junctions. *Nat. Commun.* **9**, 663 (2018).

32 Perrissin, N. *et al.* A highly thermally stable sub-20 nm magnetic random-access memory based on perpendicular shape anisotropy. *Nanoscale* **10**, 12187-12195 (2018).

33 Maruyama, T. *et al.* Large Voltage-Induced Magnetic Anisotropy Change in a Few Atomic Layers of Iron. *Nat. Nanotechnol.* **4**, 158-161 (2009).

34 Wang, W.-G., Li, M., Hageman, S. & Chien, C. Electric-field-assisted switching in magnetic tunnel junctions. *Nat. Mater.* **11**, 64-68 (2012).

35 Shiota, Y. *et al.* Induction of coherent magnetization switching in a few atomic layers of FeCo using voltage pulses. *Nat. Mater.* **11**, 39-43 (2012).

36 Ohsawa, Y. *et al.* Precise damage observation in ion-beam etched MTJ. *IEEE Trans. Magn.* **52**, 16105047 (2016).

37 Safeer, C. *et al.* Spin–orbit torque magnetization switching controlled by geometry. *Nat. Nanotechnol.* **11**, 143-146 (2016).

38 Lee, J. M. *et al.* Field-free spin–orbit torque switching from geometrical domain-wall pinning. *Nano Lett.* **18**, 4669-4674 (2018).

39 Aradhya, S. V., Rowlands, G. E., Oh, J., Ralph, D. C. & Buhrman, R. A. Nanosecond-timescale low energy switching of in-plane magnetic tunnel junctions through dynamic Oersted-field-assisted spin Hall effect. *Nano Lett.* **16**, 5987-5992 (2016).

40 Oh, Y.-W. *et al.* Field-free switching of perpendicular magnetization through spin–orbit torque in antiferromagnet/ferromagnet/oxide structures. *Nat. Nanotechnol.* **11**, 878-884 (2016).

41 Fukami, S., Zhang, C., DuttaGupta, S., Kurenkov, A. & Ohno, H. Magnetization switching by spin–orbit torque in an antiferromagnet–ferromagnet bilayer system. *Nat. Mater.* **15**, 535-541 (2016).

42 Garello, K. *et al.* Manufacturable 300mm platform solution for field-free switching SOT-MRAM. *Symposium on VLSI Circuits*, 18852132 (2019).

43 Gibertini, M., Koperski, M., Morpurgo, A. F. & Novoselov, K. S. Magnetic 2D materials and heterostructures. *Nat. Nanotechnol.* **14**, 408-419 (2019).

44 Mak, K. F., Shan, J. & Ralph, D. C. Probing and controlling magnetic states in 2D layered magnetic materials. *Nat. Rev. Phys.* **1**, 646-661 (2019).

45 Zhang, L., Zhou, J., Li, H., Shen, L. & Feng, Y. P. Recent progress and challenges in magnetic tunnel junctions with 2D materials for spintronic applications. *Appl. Phys. Rev.* **8**, 021308 (2021).

46 Och, M., Martin, M.-B., Dlubak, B., Seneor, P. & Mattevi, C. Synthesis of emerging 2D layered magnetic materials. *Nanoscale* **13**, 2157-2180 (2021).

47 Lee, K. *et al.* 22-nm FD-SOI embedded MRAM technology for low-power automotive-grade-l MCU applications. *IEEE International Electron Devices Meeting (IEDM)* **27.1**, 18437874 (2018).

48 Djayaprawira, D. D. *et al.* 230% room-temperature magnetoresistance in CoFeB/MgO/CoFeB magnetic tunnel junctions. *Appl. Phys. Lett.* **86**, 092502 (2005).

49 Vo-Van, C. *et al.* Ultrathin epitaxial cobalt films on graphene for spintronic investigations and applications. *New J. Phys.* **12**, 103040 (2010).

This work reported PMA of Co on graphene.

50 Rougemaille, N. *et al.* Perpendicular magnetic anisotropy of cobalt films intercalated under graphene. *Appl. Phys. Lett.* **101**, 142403 (2012).

51 Yang, H. *et al.* Anatomy and giant enhancement of the perpendicular magnetic anisotropy of cobalt–graphene heterostructures. *Nano Lett.* **16**, 145-151 (2016).

52 Gargiani, P., Cuadrado, R., Vasili, H. B., Pruneda, M. & Valvidares, M. Graphene-based synthetic antiferromagnets and ferrimagnets. *Nat. Commun.* **8**, 699 (2017).

53 Naganuma, H. *et al.* A perpendicular graphene/ferromagnet electrode for spintronics. *Appl. Phys. Lett.* **116**, 173101 (2020).

54 Naganuma, H. *et al.* Unveiling a Chemisorbed Crystallographically Heterogeneous Graphene/L10-FePd Interface with a Robust and Perpendicular Orbital Moment. *ACS Nano* **16**, 4139-4151 (2022).

55 Li, W., Xue, L., Abruña, H. & Ralph, D. Magnetic tunnel junctions with single-layer-graphene tunnel barriers. *Phys. Rev. B* **89**, 184418 (2014).

56 Yang, H. *et al.* Significant Dzyaloshinskii–Moriya interaction at graphene–ferromagnet interfaces due to the Rashba effect. *Nat. Mater.* **17**, 605-609 (2018).

57 Jang, P.-H., Song, K., Lee, S.-J., Lee, S.-W. & Lee, K.-J. Detrimental effect of interfacial Dzyaloshinskii-Moriya interaction on perpendicular spin-transfer-torque magnetic random access memory. *Appl. Phys. Lett.* **107**, 202401 (2015).

58 Legrand, W., Ramaswamy, R., Mishra, R. & Yang, H. Coherent subnanosecond switching of perpendicular magnetization by the fieldlike spin-orbit torque without an external magnetic field. *Phys. Rev. Appl.* **3**, 064012 (2015).

59 Sampaio, J. *et al.* Disruptive effect of Dzyaloshinskii-Moriya interaction on the magnetic memory cell performance. *Appl. Phys. Lett.* **108**, 112403 (2016).

60 Lee, O. *et al.* Central role of domain wall depinning for perpendicular magnetization switching driven by spin torque from the spin Hall effect. *Phys. Rev. B* **89**, 024418 (2014).

61 Karpan, V. M., Khomyakov, P. A., Giovannetti, G., Starikov, A. A. & Kelly, P. J. Ni (111)| graphene| h-BN junctions as ideal spin injectors. *Phys. Rev. B* **84**, 153406 (2011).

62 Bunch, J. S. *et al.* Impermeable atomic membranes from graphene sheets. *Nano lett.* **8**, 2458-2462 (2008).

63 Berry, V. Impermeability of graphene and its applications. *Carbon* **62**, 1-10 (2013).

64 Chen, S. *et al.* Oxidation resistance of graphene-coated Cu and Cu/Ni alloy. *ACS Nano* **5**, 1321-1327 (2011).

65 Hsieh, Y.-P. *et al.* Complete corrosion inhibition through graphene defect passivation. *ACS Nano* **8**, 443-448 (2014).

66 Dlubak, B. *et al.* Graphene-passivated nickel as an oxidation-resistant electrode for spintronics. *ACS Nano* **6**, 10930-10934 (2012).

67 Martin, M.-B. *et al.* Protecting nickel with graphene spin-filtering membranes: A single layer is enough. *Appl. Phys. Lett.* **107**, 012408 (2015).

68 Galbiati, M. *et al.* Spinterface: Crafting spintronics at the molecular scale. *MRS Bull.* **39**, 602 (2014).

69 Cuchet, L. *et al.* Influence of a Ta spacer on the magnetic and transport properties of perpendicular magnetic tunnel junctions. *Appl. Phys. Lett.* **103**, 052402 (2013).

70 Lee, T. Y., Won, Y. C., Lim, S. H. & Lee, S.-R. Formation of a bcc (001)-textured CoFe layer by the insertion of an FeZr layer in multilayer-based stacks with perpendicular magnetic anisotropy. *Appl. Phys. Exp.* **7**, 063002 (2014).

71 Weatherup, R. S., Dlubak, B. & Hofmann, S. Kinetic control of catalytic CVD for high-quality graphene at low temperatures. *ACS Nano* **6**, 9996-10003 (2012).

72 Dahal, A. & Batzill, M. Graphene–nickel interfaces: a review. *Nanoscale* **6**, 2548-2562 (2014).

73 Caneva, S. *et al.* Nucleation control for large, single crystalline domains of monolayer hexagonal boron nitride via Si-doped Fe catalysts. *Nano Lett.* **15**, 1867-1875 (2015).

74 Piquemal-Banci, M. *et al.* Magnetic tunnel junctions with monolayer hexagonal boron nitride tunnel barriers. *Appl. Phys. Lett.* **108**, 102404 (2016).

75 Dedkov, Y. S., Fonin, M. & Laubschat, C. A possible source of spin-polarized electrons: The inert graphene/Ni (111) system. *Appl. Phys. Lett.* **92**, 052506 (2008).

76 Piquemal-Banci, M. I. *et al.* Insulator-to-metallic spin-filtering in 2D-magnetic tunnel junctions based on hexagonal boron nitride. *ACS Nano* **12**, 4712-4718 (2018).

The above work represents the first demonstration of MR > 50% from 2DM hybridized MTJs.

77 Piquemal-Banci, M. *et al.* Spin filtering by proximity effects at hybridized interfaces in spin-valves with 2D graphene barriers. *Nat. Commun.* **11**, 5670 (2020).

78 Mistry, K. *et al.* A 45nm logic technology with high-k+ metal gate transistors, strained silicon, 9 Cu interconnect layers, 193nm dry patterning, and 100% Pb-free packaging. *IEEE International Electron Devices Meeting (IEDM)*, 247-250 (2007).

79 Chau, R., Doyle, B., Datta, S., Kavalieros, J. & Zhang, K. Integrated nanoelectronics for the future. *Nat. Mater.* **6**, 810-812 (2007).

80 Martin, M.-B. *et al.* Sub-nanometer atomic layer deposition for spintronics in magnetic tunnel junctions based on graphene spin-filtering membranes. *ACS Nano* **8**, 7890-7895 (2014).

81 Kern, L.-M. *et al.* Atomic layer deposition of a MgO barrier for a passivated black phosphorus spintronics platform. *Appl. Phys. Lett.* **114**, 053107 (2019).

82 Soluyanov, A. A. *et al.* Type-ii weyl semimetals. *Nature* **527**, 495-498 (2015).

83 Sun, Y., Wu, S.-C., Ali, M. N., Felser, C. & Yan, B. Prediction of Weyl semimetal in orthorhombic $MoTe_2$. *Phys. Rev. B* **92**, 161107 (2015).

84 Hasan, M. Z. & Kane, C. L. Colloquium: topological insulators. *Rev. Mod. Phys.* **82**, 3045 (2010).

85 Gong, C. *et al.* Discovery of intrinsic ferromagnetism in two-dimensional van der Waals crystals. *Nature* **546**, 265-269 (2017).

86 Huang, B. *et al.* Layer-dependent ferromagnetism in a van der Waals crystal down to the monolayer limit. *Nature* **546**, 270-273 (2017).

The above two papers first reported two-dimensional vdW ferromagnets.

87 Deng, Y. *et al.* Gate-tunable room-temperature ferromagnetism in two-dimensional Fe_3GeTe_2. *Nature* **563**, 94-99 (2018).

This work showed gate tunable room temperature ferromagnetism in 2D Fe_3GeTe_2.

88 Freitas, D. C. *et al.* Ferromagnetism in layered metastable 1T-CrTe2. *J. Phys. Condens. Matter* **27**, 176002 (2015).

89 Costa, J. *et al.* Impact of MgO thickness on the performance of spin-transfer torque nano-oscillators. *IEEE Trans. Magn.* **51**, 15552723 (2015).

90 Sato, S. *et al.* Study on initial current leakage spots in CoFeB-capped MgO tunnel barrier by

conductive atomic force microscopy. *Jpn. J. Appl. Phys.* **55**, 04EE05 (2016).

91 Karpan, V. *et al.* Graphite and graphene as perfect spin filters. *Phys. Rev. Lett.* **99**, 176602 (2007).

This is a seminal paper on the potential of 2D materials (here graphene) for spin filtering in MTJs.

92 Piquemal-Banci, M. *et al.* 2D-MTJs: introducing 2D materials in magnetic tunnel junctions. *J. Phys. D: Appl. Phys.* **50**, 203002 (2017).

93 Novoselov, K., Mishchenko, A., Carvalho, A. & Neto, A. C. 2D materials and van der Waals heterostructures. *Science* **353**, aac9439 (2016).

94 Kang, K. *et al.* Layer-by-layer assembly of two-dimensional materials into wafer-scale heterostructures. *Nature* **550**, 229-233 (2017).

95 Yazyev, O. V. & Pasquarello, A. Magnetoresistive junctions based on epitaxial graphene and hexagonal boron nitride. *Phys. Rev. B* **80**, 035408 (2009).

96 Lazić, P., Sipahi, G., Kawakami, R. & Žutić, I. Graphene spintronics: Spin injection and proximity effects from first principles. *Phys. Rev. B* **90**, 085429 (2014).

97 Cobas, E., Friedman, A. L., van't Erve, O. M., Robinson, J. T. & Jonker, B. T. Graphene as a tunnel barrier: graphene-based magnetic tunnel junctions. *Nano Lett.* **12**, 3000-3004 (2012).

98 Asshoff, P. U. *et al.* Magnetoresistance in Co-hBN-NiFe tunnel junctions enhanced by resonant tunneling through single defects in ultrathin hBN barriers. *Nano Lett.* **18**, 6954-6960 (2018).

99 Wang, Z. *et al.* Tunneling spin valves based on Fe_3GeTe_2/hBN/Fe_3GeTe_2 van der Waals heterostructures. *Nano Lett.* **18**, 4303-4308 (2018).

This work reported the realization of MTJ based on vdW heterostructures.

100 Dankert, A. & Dash, S. P. Electrical gate control of spin current in van der Waals heterostructures at room temperature. *Nat. Commun.* **8**, 16093 (2017).

101 Zatko, V. *et al.* Band-structure spin-filtering in vertical spin valves based on chemical vapor deposited WS_2. *ACS Nano* **13**, 14468-14476 (2019).

102 Yan, Z., Zhang, R., Dong, X., Qi, S. & Xu, X. Significant tunneling magnetoresistance and excellent filtering effect in CrI_3-based Van der Waals magnetic tunnel junctions. *Phys. Chem. Chem. Phys* **22**, 14773-14780 (2020).

103 Mohiuddin, T. M. *et al.* Graphene in multilayered CPP spin valves. *IEEE Trans. Magn.* **44**, 10362084 (2008).

104 Godel, F. *et al.* Voltage-controlled inversion of tunnel magnetoresistance in epitaxial nickel/graphene/MgO/cobalt junctions. *Appl. Phys. Lett.* **105**, 152407 (2014).

105 Iqbal, M. Z., Iqbal, M. W., Siddique, S., Khan, M. F. & Ramay, S. M. Room temperature spin valve effect in NiFe/WS_2/Co junctions. *Sci. Rep.* **6**, 21038 (2016).

106 Dankert, A. *et al.* Spin-polarized tunneling through chemical vapor deposited multilayer molybdenum disulfide. *ACS Nano* **11**, 6389-6395 (2017).

107 Entani, S. *et al.* Magnetoresistance effect in $Fe_{20}Ni_{80}$/graphene/$Fe_{20}Ni_{80}$ vertical spin valves. *Appl. Phys. Lett.* **109**, 082406 (2016).

108 Caneva, S. *et al.* Controlling catalyst bulk reservoir effects for monolayer hexagonal boron nitride CVD. *Nano Lett.* **16**, 1250-1261 (2016).

109 Reale, F. *et al.* High-mobility and high-optical quality atomically thin WS_2. *Sci. Rep.* **7**, 14911 (2017).

110 Zhou, J. *et al.* A library of atomically thin metal chalcogenides. *Nature* **556**, 355-359 (2018).

111 Loh, T. A., Chua, D. H. & Wee, A. T. One-step synthesis of few-layer WS_2 by pulsed laser deposition. *Sci. Rep.* **5**, 18116 (2015).

112 Nakano, M., Wang, Y., Kashiwabara, Y., Matsuoka, H. & Iwasa, Y. Layer-by-layer epitaxial growth of scalable WSe2 on sapphire by molecular beam epitaxy. *Nano Lett.* **17**, 5595-5599 (2017).

113 Godel, F. *et al.* WS_2 2D Semiconductor Down to Monolayers by Pulsed-Laser Deposition for Large-Scale Integration in Electronics and Spintronics Circuits. *ACS Appl. Nano Mater.* **3**, 7908-7916 (2020).

114 Zatko, V. *et al.* Band-Gap Landscape Engineering in Large-Scale 2D Semiconductor van der Waals Heterostructures. *ACS Nano* **15**, 7279–7289 (2021).

This work represents the first demonstration of tunnelling barrier band-gap engineering for MTJs.

115 Yuasa, S., Nagahama, T., Fukushima, A., Suzuki, Y. & Ando, K. Giant room-temperature magnetoresistance in single-crystal Fe/MgO/Fe magnetic tunnel junctions. *Nat. Mater.* **3**, 868-871 (2004).

116 Parkin, S. S. *et al.* Giant tunnelling magnetoresistance at room temperature with MgO (100) tunnel barriers. *Nat. Mater.* **3**, 862-867 (2004).

117 Li, X. *et al.* Spin-dependent transport in van der Waals magnetic tunnel junctions with Fe_3GeTe_2 electrodes. *Nano Lett.* **19**, 5133-5139 (2019).

118 Klein, D. R. *et al.* Probing magnetism in 2D van der Waals crystalline insulators via electron tunneling. *Science* **360**, 1218-1222 (2018).

119 Song, T. *et al.* Giant tunneling magnetoresistance in spin-filter van der Waals heterostructures. *Science* **360**, 1214-1218 (2018).

The above two works reported MTJs based on vdW heterostructures in which atomically thin CrI_3 acts as a spin-filter tunnel barrier.

120 Yang, W. *et al.* Spin-filter induced large magnetoresistance in 2D van der Waals magnetic tunnel junctions. *Nanoscale* **13**, 862-868 (2021).

121 Grimaldi, E. *et al.* Single-shot dynamics of spin–orbit torque and spin transfer torque switching in three-terminal magnetic tunnel junctions. *Nat. Nanotechnol.* **15**, 111-117 (2020).

122 Gupta, M. *et al.* High-density SOT-MRAM technology and design specifications for the embedded domain at 5nm node. *IEEE International Electron Devices Meeting (IEDM)* **24.5**, 20548648 (2020).

123 Ramaswamy, R., Lee, J. M., Cai, K. & Yang, H. Recent advances in spin-orbit torques: Moving towards device applications. *Appl. Phys. Rev.* **5**, 031107 (2018).

124 Shao, Q. *et al.* Roadmap of spin-orbit torques. *IEEE Trans. Magn.* **57**, 800439 (2021).

125 Han, J. *et al.* Room-temperature spin-orbit torque switching induced by a topological insulator. *Phys. Rev. Lett.* **119**, 077702 (2017).

126 Wang, Y. *et al.* Room temperature magnetization switching in topological insulator-ferromagnet heterostructures by spin-orbit torques. *Nat. Commun.* **8**, 1364 (2017).

The above two papers reported room temperature SOT switching by a topological insulator.

127 Shi, S. *et al.* All-electric magnetization switching and Dzyaloshinskii–Moriya interaction in WTe_2/ferromagnet heterostructures. *Nat. Nanotechnol.* **14**, 945-949 (2019).

The first SOT switching report by a Weyl semimetal spin current source.

128 MacNeill, D. *et al.* Control of spin–orbit torques through crystal symmetry in WTe_2/ferromagnet bilayers. *Nat. Phys.* **13**, 300-305 (2017).

The first experimental report to generate an out-of-plane antidamping torque using TMDC.

129 Li, X. *et al.* Large and robust charge-to-spin conversion in sputtered Weyl semimetal WTex with structural disorder. Preprint at https://arxiv-org.libproxy1.nus.edu.sg/abs/2001.04054 (2020).

130 Shi, S. *et al.* Observation of the Out-of-Plane Polarized Spin Current from CVD Grown WTe_2. *Adv. Quantum Technol.* **4**, 2100038 (2021).

131 Alghamdi, M. *et al.* Highly efficient spin–orbit torque and switching of layered ferromagnet Fe_3GeTe_2. *Nano Lett.* **19**, 4400-4405 (2019).

132 Wang, X. *et al.* Current-driven magnetization switching in a van der Waals ferromagnet Fe_3GeTe_2. *Sci. Adv.* **5**, eaaw8904 (2019).

The above two works demonstrated spin current induced magnetization switching in a vdW ferromagnet.

133 Gupta, V. *et al.* Manipulation of the van der Waals Magnet $Cr_2Ge_2Te_6$ by Spin–Orbit Torques. *Nano Lett.* **20**, 7482-7488 (2020).

134 Ostwal, V., Shen, T. & Appenzeller, J. Efficient Spin-Orbit Torque Switching of the Semiconducting Van Der Waals Ferromagnet $Cr_2Ge_2Te_6$. *Adv. Mater.* **32**, 1906021 (2020).

135 Lv, W. *et al.* Electric-Field Control of Spin–Orbit Torques in WS_2/Permalloy Bilayers. *ACS Appl. Mater. Inter.* **10**, 2843-2849 (2018).

136 Shao, Q. *et al.* Strong Rashba-Edelstein effect-induced spin–orbit torques in monolayer transition metal dichalcogenide/ferromagnet bilayers. *Nano Lett.* **16**, 7514-7520 (2016).

137 Shao, Y. *et al.* The current modulation of anomalous Hall effect in van der Waals Fe_3GeTe_2/WTe_2 heterostructures. *Appl. Phys. Lett.* **116**, 092401 (2020).

138 Shin, I. *et al.* Spin-orbit Torque Switching in an All-Van der Waals Heterostructure. *Adv. Mater.* **34**, 2101730 (2022).

139 Loong, L. M. *et al.* Strain-enhanced tunneling magnetoresistance in MgO magnetic tunnel junctions. *Sci. Rep.* **4**, 6505 (2014).

140 Dai, Z., Liu, L. & Zhang, Z. Strain engineering of 2D materials: issues and opportunities at the interface. *Adv. Mat.* **31**, 1805417 (2019).

141 Loong, L. M. *et al.* Flexible MgO barrier magnetic tunnel junctions. *Adv. Mater.* **28**, 4983 (2016).

142 Sahadevan, A. M. *et al.* Biaxial strain effect of spin dependent tunneling in MgO magnetic tunnel junctions. *Appl. Phys. Lett.* **101**, 042407 (2012).

143 Žutić, I., Matos-Abiague, A., Scharf, B., Dery, H. & Belashchenko, K. Proximitized materials. *Mater. Today* **22**, 85-107 (2019).

144 Benítez, L. A. *et al.* Tunable room-temperature spin galvanic and spin Hall effects in van der Waals heterostructures. *Nat. Mater.* **19**, 170-175 (2020).

This work is the first demonstration of gate-tunable spin Hall and spin galvanic effects at room temperature.

145 Jung, S. *et al.* A crossbar array of magnetoresistive memory devices for in-memory computing. *Nature* **601**, 211-216 (2022).

This work is the first report of in-memory computing using MRAM devices.

146 Choi, S. H. *et al.* Large-scale synthesis of graphene and other 2D materials towards industrialization. *Nat. Commun.* **13**, 1484 (2022).

147 Lemme, M. C., Akinwande, D., Huyghebaert, C. & Stampfer, C. 2D materials for future heterogeneous electronics. *Nat. Commun.* **13**, 1392, doi:10.1038/s41467-022-29001-4 (2022).

148 Ren, Y., Qiao, Z. & Niu, Q. Topological phases in two-dimensional materials: a review. *Rep. Prog. Phys.* **79**, 066501 (2016).

149 Fiori, G. *et al.* Electronics based on two-dimensional materials. *Nat. Nanotechnol.* **9**, 768-779 (2014).

150 Xu, M., Liang, T., Shi, M. & Chen, H. Graphene-like two-dimensional materials. *Chem. Rev.* **113**, 3766-3798 (2013).

151 Bowen, M. *et al.* Large magnetoresistance in Fe/MgO/FeCo(001) epitaxial tunnel junctions on GaAs(001). *Appl. Phys. Lett.* **79**, 1655-1657 (2001).

152 O'Hara, D. J. *et al.* Room temperature intrinsic ferromagnetism in epitaxial manganese selenide films in the monolayer limit. *Nano Lett.* **18**, 3125-3131 (2018).

153 Li, B. *et al.* A two-dimensional Fe-doped SnS_2 magnetic semiconductor. *Nat. Commun.* **8**, 1958 (2017).

154 Dau, M. *et al.* van der Waals epitaxy of Mn-doped $MoSe_2$ on mica. *APL Mater.* **7**, 051111 (2019).

155 Bonilla, M. *et al.* Strong room-temperature ferromagnetism in VSe_2 monolayers on van der Waals substrates. *Nat. Nanotechnol.* **13**, 289-293 (2018).

156 Lopes, J. M. J. *et al.* Large-area van der Waals epitaxy and magnetic characterization of Fe_3GeTe_2 films on graphene. *2D Mater.* **8**, 041001 (2021).

157 Ribeiro, M. *et al.* Large-scale epitaxy of two-dimensional van der Waals room-temperature ferromagnet Fe_5GeTe_2. *npj 2D Mater. Appl* **6**, 10 (2022).

158 Walsh, L. A. *et al.* Interface chemistry of contact metals and ferromagnets on the topological insulator Bi_2Se_3. *J. Phys. Chem. C* **121**, 23551-23563 (2017).

159 Galbiati, M. *et al.* Path to Overcome Material and Fundamental Obstacles in Spin Valves

Based on MoS_2 and Other Transition-Metal Dichalcogenides. *Phys. Rev. Appl.* **12**, 044022 (2019).

160 Bonell, F. *et al.* Control of spin-orbit torques by interface engineering in topological insulator heterostructures. *Nano Lett.* **20**, 5893-5899 (2020).

161 Zhu, D. *et al.* Highly efficient charge-to-spin conversion from in situ Bi_2Se_3/Fe heterostructures. *Appl. Phys. Lett.* **118**, 062403 (2021).

162 Dau, M. T. *et al.* Beyond van der Waals interaction: the case of $MoSe_2$ epitaxially grown on few-layer graphene. *ACS Nano* **12**, 2319-2331 (2018).

163 Dau, M. T. *et al.* The valley Nernst effect in WSe_2. *Nat. Commun.* **10**, 5796 (2019).

164 Mallet, P. *et al.* Bound Hole States Associated to Individual Vanadium Atoms Incorporated into Monolayer WSe_2. *Phys. Rev. Lett.* **125**, 036802 (2020).

165 Cai, Z., Liu, B., Zou, X. & Cheng, H.-M. Chemical vapor deposition growth and applications of two-dimensional materials and their heterostructures. *Chem. Rev.* **118**, 6091-6133 (2018).

166 Nicolosi, V., Chhowalla, M., Kanatzidis, M. G., Strano, M. S. & Coleman, J. N. Liquid exfoliation of layered materials. *Science* **340**, 1226419 (2013).

167 Yao, J., Zheng, Z. & Yang, G. Production of large-area 2D materials for high-performance photodetectors by pulsed-laser deposition. *Prog. Mater. Sci* **106**, 100573 (2019).

168 Yang, Z. & Hao, J. Progress in pulsed laser deposited two-dimensional layered materials for device applications. *J. Mater. Chem. C* **4**, 8859-8878 (2016).

169 Tao, J. *et al.* Growth of wafer-scale MoS_2 monolayer by magnetron sputtering. *Nanoscale* **7**, 2497-2503 (2015).

170 Lee, J.-H. *et al.* Wafer-scale growth of single-crystal monolayer graphene on reusable hydrogen-terminated germanium. *Science* **344**, 286-289 (2014).

171 Lee, J. S. *et al.* Wafer-scale single-crystal hexagonal boron nitride film via self-collimated grain formation. *Science* **362**, 817-821 (2018).

172 Wang, L. *et al.* Epitaxial growth of a 100-square-centimetre single-crystal hexagonal boron nitride monolayer on copper. *Nature* **570**, 91-95 (2019).

173 Kim, J., Sakakita, H. & Itagaki, H. J. N. l. Low-temperature graphene growth by forced convection of plasma-excited radicals. *Nano Lett.* **19**, 739-746 (2019).

174 Lee, C. S. *et al.* Fabrication of metal/graphene hybrid interconnects by direct graphene growth and their integration properties. *Adv. Electron. Mater.* **4**, 1700624 (2018).

175 Seol, M. *et al.* High-Throughput Growth of Wafer-Scale Monolayer Transition Metal Dichalcogenide via Vertical Ostwald Ripening. *Adv. Mater.* **32**, 2003542 (2020).

176 Kang, K. *et al.* High-mobility three-atom-thick semiconducting films with wafer-scale homogeneity. *Nature* **520**, 656-660 (2015).

177 Delabie, A. *et al.* Low temperature deposition of 2D WS_2 layers from WF_6 and H_2S precursors: impact of reducing agents. *Chem. Commun.* **51**, 15692-15695 (2015).

178 Reina, A. *et al.* Large area, few-layer graphene films on arbitrary substrates by chemical vapor deposition. *Nano Lett.* **9**, 30-35 (2009).

This work reported the first polymer-assisted transfer.

179 Lee, Y. *et al.* Wafer-scale synthesis and transfer of graphene films. *Nano Lett.* **10**, 490-493 (2010).

180 Bae, S. *et al.* Roll-to-roll production of 30-inch graphene films for transparent electrodes. *Nat. Nanotechnol.* **5**, 574-578 (2010).

The above two papers showed a wafer scale transfer of 2DM using polymer and thermal release tape.

181 Shim, J. *et al.* Controlled crack propagation for atomic precision handling of wafer-scale two-dimensional materials. *Science* **362**, 665-670 (2018).

182 Liu, F. *et al.* Disassembling 2D van der Waals crystals into macroscopic monolayers and reassembling into artificial lattices. *Science* **367**, 903-906 (2020).

183 Shin, Y. J. *et al.* Surface-energy engineering of graphene. *Langmuir* **26**, 3798-3802 (2010).

184 Brennan, C. J., Nguyen, J., Yu, E. T. & Lu, N. Interface adhesion between 2D materials and elastomers measured by buckle delaminations. *Adv. Mater. Interfaces* **2**, 1500176 (2015).

185 Chen, P. Y., Liu, M., Wang, Z., Hurt, R. H. & Wong, I. Y. From Flatland to Spaceland: Higher Dimensional Patterning with Two-Dimensional Materials. *Adv. Mat.* **29**, 1605096 (2017).

186 He, T. *et al.* Etching techniques in 2D materials. *Adv. Mat. Technologies* **4**, 1900064 (2019).

187 Cai, X., Luo, Y., Liu, B. & Cheng, H.-M. Preparation of 2D material dispersions and their applications. *Chem. Soc. Rev.* **47**, 6224-6266 (2018).

188 Qiu, X. P. *et al.* Disorder-free sputtering method on graphene. *AIP Adv.* **2**, 032121 (2012).

189 Lee, T. Y. *et al.* Magnetic immunity guideline for embedded MRAM reliability to realize mass production. *IEEE International Reliability Physics Symposium (IRPS)* **7A. 2** 19745115 (2020).

190 Srivastava, S. *et al.* Magnetic immunity of spin-transfer-torque MRAM. *Appl. Phys. Lett.* **114**, 172405 (2019).

191 Lee, T. Y. *et al.* Fast switching of STT-MRAM to realize high speed applications. *IEEE Symposium on VSLI Technology* 20237276 (2020).

192 Cubukcu, M. *et al.* Ultra-fast perpendicular spin–orbit torque MRAM. *IEEE Trans. Magn.* **54**, 17618500 (2018).

193 Lee, J. M. *et al.* Oscillatory spin-orbit torque switching induced by field-like torques. *Comm. Phys.* **1**, 2 (2018).

194 Krizakova, V., Garello, K., Grimaldi, E., Kar, G. S. & Gambardella, P. J. A. P. L. Field-free switching of magnetic tunnel junctions driven by spin–orbit torques at sub-ns timescales. *Appl. Phys. Lett.* **116**, 232406 (2020).

195 Kato, Y. *et al.* Improvement of Write Efficiency in Voltage-Controlled Spintronic Memory by development of a Ta−B Spin Hall Electrode. *Phys. Rev. Appl.* **10**, 044011 (2018).

196 Graphene Flagship. *The 2D Experimental Pilot line is an initiative launched by the Graphene Flagship*, <https://www.graphene-flagship.eu/innovation/pilot-line/> (2020).

197 Mishra, R. & Yang, H. Emerging spintronics phenomena and applications. *IEEE Trans. Magn.* **57**, 0800134 (2020).

198 Huyghebaert, C. *et al.* 2D materials: Roadmap to CMOS integration. *IEEE International Electron Devices Meeting (IEDM)* **22.1**, 18420807 (2018).

199 MarketWatch. *Microcontrollers (MCU) Market Trend 2021, Industry Size, Company Share, Leading Top Countries with Recent Development, Manufacturing Cost Analysis, Revenues, Estimates and Forecast to 2027*, <https://www.marketwatch.com/press-release/microcontrollers-mcu-market-trend-2021-industry-size-company-share-leading-top-countries-with-recent-development-manufacturing-cost-analysis-revenues-estimates-and-forecast-to-2027-2021-08-11> (2021).

200 Jabeur, K., Di Pendina, G. & Prenat, G. Ultra-energy-efficient CMOS/magnetic non-volatile flip-flop based on spin-orbit torque device. *Electron. lett.* **50**, 585-587 (2014).

201 Moradi, F. *et al.* Spin-Orbit-Torque-based Devices, Circuits and Architectures. Preprint at https://arxiv-org.libproxy1.nus.edu.sg/abs/1912.01347v01341 (2019).

202 He, Z., Angizi, S., Parveen, F. & Fan, D. High performance and energy-efficient in-memory computing architecture based on SOT-MRAM. *IEEE/ACM International Symposium on Nanoscale Architectures (NANOARCH)*, 17215732 (2017).

203 Bertolazzi, S. *MRAM Technology and Market Trends*, <https://www.flashmemorysummit.com/Proceedings2019/08-05-Monday/20190805_MRAMDD_Plenary_Bertolazzi.pdf> (2019).

204 Markets Insider. *Everspin begins 40 nm STT-MRAM volume production*, <https://markets.businessinsider.com/news/stocks/everspin-begins-40nm-stt-mram-volume-production-1013155489> (2018).

205 Everspin Technologies Inc. *Everspin Enters Pilot Production Phase for the World's First 28 nm 1 Gb STT-MRAM Component*, <https://www.everspin.com/news/everspin-enters-pilot-production-phase-world%E2%80%99s-first-28-nm-1-gb-stt-mram-component> (2019).

206 AnandTech. *Samsung Ships First Commercial Embedded MRAM (eMRAM) Product*, <https://www.anandtech.com/show/14056/samsung-ships-first-commercial-emram-product> (2019).

207 GLOBALFOUNDRIES. *GLOBALFOUNDRIES Delivers Industry's First Production-ready eMRAM on 22FDX Platform for IoT and Automotive Applications*, <https://www.globalfoundries.com/news-events/press-releases/globalfoundries-delivers-industrys-first-production-ready-emram-22fdx> (2020).

208 Golonzka, O. *et al.* MRAM as embedded non-volatile memory solution for 22FFL FinFET technology. *IEEE International Electron Devices Meeting (IEDM)* **18.1**, 18420890 (2018).

Acknowledgements

M.C., A.F., K.G., P.S., S.O.V. and S.R. acknowledge the European Union Horizon 2020 research and innovation program for grant number 881603 (Graphene Flagship). The Catalan Institute of Nanoscience and Nanotechnology is supported by the Severo Ochoa Centres of Excellence program, funded by the Spanish Research Agency (AEI, grant no. SEV-2017-0706). S.O.V. thanks the European Research Council (ERC) under Grant Agreements 306652 SPINBOUND and 899896 SOTMEM and the Spanish Research Agency (AEI), Ministry of Science and Innovation (PID2019-111773RB-I00/AEI/10.13039/501100011033). H.Y. is supported by SpOT-LITE program (A*STAR grant, A18A6b0057) through RIE2020 funds, Singapore Ministry of Education (MOE) Tier 1 (R263-000-D61-114), National Research Foundation (NRF) Singapore Investigatorship (NRFI06-2020-0015) and Samsung Electronics' University R&D program. S.C. and G.S.K. acknowledge IMEC's Industrial Affiliation Program on MRAM devices. M.C. and M.J. acknowledge the French National Research Agency through the MAGICVALLEY project (ANR-18-CE24-0007). B.D. acknowledges ERC MAGICAL 669204. M.C. acknowledges H.X. Yang, A. Hallal, F. Ibrahim. P.S. and B.D. acknowledge the French National Research Agency through the SoGraphMem project (ANR-18-CE24-0007).

Author contributions

All authors wrote and commented on the manuscript.

Competing interests The authors declare no competing interests.

Additional information

Reprints and permissions information is available at http://www.nature.com/reprints.

Correspondence and requests for materials should be addressed to H.Y. (eleyang@nus.edu.sg), S.O.V. (SOV@icrea.cat) or S.R. (stephan.roche@icn2.cat).